Journal of Alloys and Compounds 675 (2016) 355–363

Contents lists available at ScienceDirect

Journal of Alloys and Compounds

journal homepage: http://www.elsevier.com/locate/jalcom

Strong second harmonic generation in $LiInX_2$ (X=Se, Te) chalcopyrite crystals as explored by first-principles methods

A.H. Reshak [a, b, *], M.G. Brik [c, d, e]

[a] New Technologies - Research Centre, University of West Bohemia, Univerzitni 8, 306 14 Pilsen, Czech Republic
[b] Center of Excellence Geopolymer and Green Technology, School of Material Engineering, University Malaysia Perlis, 01007 Kangar, Perlis, Malaysia
[c] College of Sciences, Chongqing University of Posts and Telecommunications, Chongqing 400065, PR China
[d] Institute of Physics, University of Tartu, Ravila 14C, Tartu 50411, Estonia
[e] Institute of Physics, Jan Dlugosz University, Armii Krajowej 13/15, PL-42200 Czestochowa, Poland

ARTICLE INFO

Article history:
Received 20 November 2015
Received in revised form
23 February 2016
Accepted 14 March 2016
Available online 21 March 2016

Keywords:
Electronic band structure
Linear optical properties
Nonlinear optical properties
mBJ

ABSTRACT

Complex first-order linear optical dispersion and complex second-order non-linear optical dispersion of $LiInX_2$ (X = Se, Te) chalcopyrite single crystals were calculated in the framework of the density functional theory using the local density approximation (LDA), general gradient approximation (GGA) and modified Becke-Johnson potential The performed calculations show that these materials posses direct energy band gap (−Γ) of about 1.58 eV (LDA), 1.85 eV (GGA) and 2.04 eV (mBJ) for $LiInSe_2$ and 1.76 eV (LDA), 1.92 eV (GGA) and 2.40 eV (mBJ) for $LiInTe_2$. Comparison with the experimental data unambiguously indicates that the mBJ succeeds by bringing the calculated gaps in close agreement with the measured ones (2.05 eV -$LiInSe_2$ and 2.41 eV -$LiInTe_2$). It has been found that both compounds exhibit negative uniaxial anisotropy and positive birefringence at the static limit. In addition, $LiInTe_2$ exhibits a higher second harmonic generation (SHG) signal than $LiInSe_2$. Moreover, $LiInSe_2$ ($LiInTe_2$) exhibits a SHG signal of about seven (nine) times greater than the corresponding experimental value for the well known $KTiOPO_4$ (KTP) single crystals.

1. Introduction

In the recent years ternary semiconducting compounds have received much attention [1–3]. The ternary chalcopyrite compounds form a large group of semiconducting materials with diverse optical, electrical and structural properties [4–11]. These compounds appear to be promising candidates for the solar-cells [12], light-emitting diodes [13], nonlinear optics [14] and optical frequency conversion applications in all solid state based tunable laser systems [15]. The ternary chalcopyrite compounds can be grown as thin films and their band gaps can vary from infrared (most of all) to ultraviolet (fewer compounds) spectral regions matching solar spectrum, which makes their applications in solar panels to be quite promising. As an illustration to the last statement, it can be mentioned that the Cu(In,Ga) $(Se,S)_2$-based solar elements already question a long dominance of the silicon-based solar panels [16]. Many research works to synthesize novel chalcopyrite materials, both neat and mixed with partial cation or anion substitution, have been reported. It was recently demonstrated that $LiInSe_2$ exhibits high potential as a solar cell material [17]. Theoretical calculations for the $LiInS_2$, $LiInSe_2$ and $LiInTe_2$ chalcopyrites were performed to analyze the lattice dynamics, thermodynamic, elastic properties [18–23].

Lagoun et al. [24] have reported the elastic and piezoelectric properties of $LiMX_2$ (M = Ga, In; X = S, Se) crystals. Recently Ma and Brik [25] reported the structural, electronic, and optical properties of $LiInSe_2$ and $LiInTe_2$ crystals using the CASTEP code within the local density approximation (LDA) and generalized gradient approximation (GGA). Special emphasis was placed upon the role of the Se and Te anions in formation of the peculiar features of the electronic and optical properties of these compounds.

At the same time it should be stressed out that there is a certain lack of information on the nonlinear optical properties of $LiInSe_2$ and $LiInTe_2$. To fill in this gap, we calculated the nonlinear optical properties of these compounds using the recently modified Becke-Johnson potential (mBJ) based on the calculated band structures within mBJ. Application of mBJallows for the calculation of the band gaps with accuracy similar to the very expensive GW calculations. It is a local approximation to an atomic “exact-exchange” potential and a screening term. The paper is organized as follows: in the next section we describe the details of calculations and crystal structure

* Corresponding author. New Technologies - Research Centre, University of West Bohemia, Univerzitni 8, 306 14 Pilsen, Czech Republic.
E-mail address: maalidph@yahoo.co.uk (A.H. Reshak).

http://dx.doi.org/10.1016/j.jallcom.2016.03.104
0925-8388/

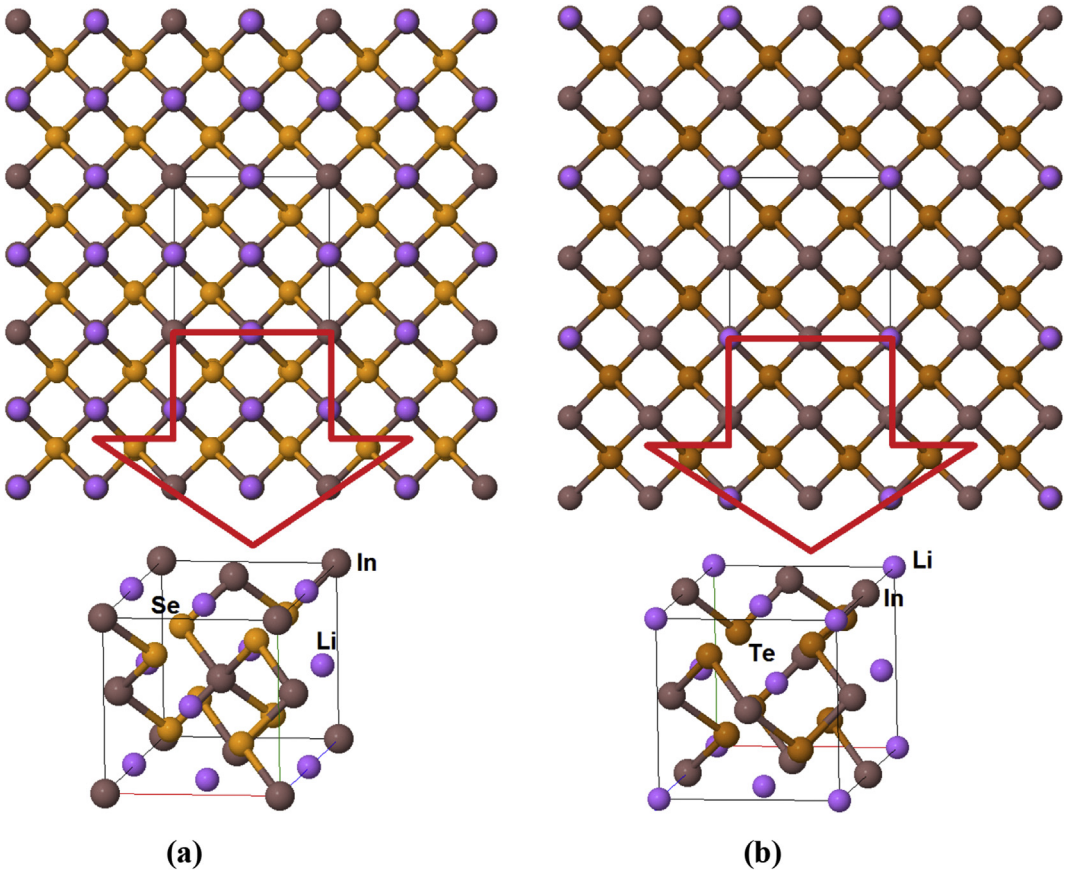

Fig. 1. Crystal structure of $LiInSe_2$ and $LiInTe_2$.

Table 1
Optimized crystal structure of $LiInSe_2$ in comparison with the experimental data [26,27] and the previous theoretical calculations [25].

Cell parameters (Å)		A		b		c
Exp.		5.807[a]		5.807[a]		11.810[a]
This work		5.823		5.823		11.796
Previous work		6.005[b]		6.005[b]		11.875[b]
		5.835[c]		5.835[c]		11.593[c]
Atomic positions						
Atom	x exp.	x optim.	y exp.	y optim.	z exp.	z optim.
In	0.0	0.0	0.0	0.0	0.0	0.0
Li	0.0	0.0	0.0	0.0	0.5	0.5
Se	0.257	0.244	0.25	0.25	0.125	0.125

[a] Ref. [26,27].
[b] Ref. Brik (GGA) [25].
[c] Ref. Brik (LDA) [25].

Table 2
Optimized crystal structure of $LiInTe_2$ in comparison with the experimental data [26,27] and the previous theoretical calculations [25].

Cell parameters (Å)		A		b		c
Exp.		6.398[a]		6.398[a]		12.460[a]
This work		6.354		6.354		12.400
Previous work		6.546[b]		6.546[b]		12.804[b]
		6.300[c]		6.300[c]		12.482[c]
Atomic positions						
atom	x exp.	x optim.	y exp.	y optim.	z exp.	z optim.
In	0.0	0.0	0.0	0.0	0.5	0.5
Li	0.0	0.0	0.0	0.0	0.0	0.0
Te	0.241	0.243	0.25	0.25	0.125	0.125

[a] Ref. [26,27].
[b] Ref. Brik (GGA) [25].
[c] Ref. Brik (LDA) [25].

of the studied samples. We proceed with the description of the calculated results and conclude the paper with a summary of the main results obtained.

2. Details of calculations

The ternary chalcopyrite compounds $LiInX_2$ (X = Se, Te) crystallize in non-centro-symmetric tetragonal space group I-42d with four formula units per one unit cell. The crystal structure of $LiInX_2$ (X = Se, Te) single crystals is illustrated in Fig. 1. The experimental lattice parameters of $LiInSe_2$ are a = b = 5.807 Å, c = 11.810 Å and Z = 4 [26], whereas the same parameters for $LiInTe_2$ are a = b = 6.398 Å, c = 12.460 Å and Z = 4 [27]. We have optimized the experimental lattice constant of $LiInX_2$ (X = Se, Te) using the LDA [28]. Calculations yield the lattice constants a = b = 5.829 Å and c = 11.738 Å for $LiInSe_2$, while for $LiInTe_2$ a = b = 6.328 Å and c = 12.422 Å, in good agreement with the experimental values [26,27]. Further the atomic positions were optimized using the generalized gradient approximation (PBE-GGA) [29] by minimizing the forces acting on the atoms. The optimized crystal structure data are listed in Tables 1 and 2 in comparison with the experimental data [26,27] and previous theoretical results [25]. The crystal structure of $LiInX_2$ (X = Se, Te) single crystals are illustrated in Fig. 1. We have used the relaxed geometrical structure to calculate the band structures and hence the complex linear and nonlinear optical susceptibilities. The all-electron full potential linear augmented plane wave plus local orbitals (FPLAPW + lo) method in a scalar relativistic version as embodied in the WIEN2k code [30] was employed in these calculations. This is an implementation of the density functional theory (DFT) with different possible approximations for the exchange-correlation (XC) potential. The exchange and correlation potentials were described by the LDA and PBE-GGA approximations, which is based on exchange-correlation energy optimization to calculate the total energy. In addition, we have used the recently modified Becke-Johnson potential (mBJ) [31], which optimizes the corresponding potential for electronic band structure calculations. The Kohn–-Sham equations are solved using a basis of linear APW's. The potential and charge density in the muffin-tin (MT) spheres are expanded in spherical harmonics with $l_{max} = 8$ and nonspherical components up to $l_{max} = 6$. In the interstitial region the potential and the charge density are represented by the Fourier series. Self-consistency of the calculated results is obtained using 500 k points in the irreducible Brillouin zone (IBZ). We have calculated the linear optical susceptibilities using 800 k points and the nonlinear optical susceptibilities using 1500 k points in the IBZ.

The non-centro-symmetric tetragonal (I-42d) symmetry allows three non-zero components of the second-order dielectric (optical) tensor corresponding to the electric field $\vec{E}$ being directed along the **a**, **b**, and **c**-crystallographic axes. These are $\varepsilon^{xx}(\omega) = \varepsilon^{yy}(\omega) = \varepsilon_2^{\perp}(\omega)$ and $\varepsilon^{zz}(\omega) = \varepsilon_2^{II}(\omega)$. The imaginary part $\varepsilon_2^{\perp}(\omega)$ and $\varepsilon_2^{II}(\omega)$ of the principal complex tensor components completely defines the linear optical susceptibilities. The imaginary part can be obtained using the following expression [32]:

$$\varepsilon_2^{ij}(\omega) = \frac{8\pi^2\hbar^2e^2}{m^2V}\sum_k\sum_{cv}(f_c - f_v)\frac{p_{cv}^i(k)p_{vc}^j(k)}{E_{vc}^2}\delta[E_c(k) - E_v(k) - \hbar\omega], \quad (1)$$

where m, e and $\hbar$ are the electron mass, charge and Planck's constant, respectively. f_c and f_v represent the Fermi distributions of the conduction and valence bands, respectively. The term $p_{cv}^i(k)$ denotes the momentum matrix element transition from the energy level c of the conduction band to the level v of the valence band at certain **k**-point in the BZ and V is the unit cell volume. The real part of the dielectric function is obtained afterwards using Kramer–Kronig relationship [33].

Furthermore, we have calculated the complex second-order

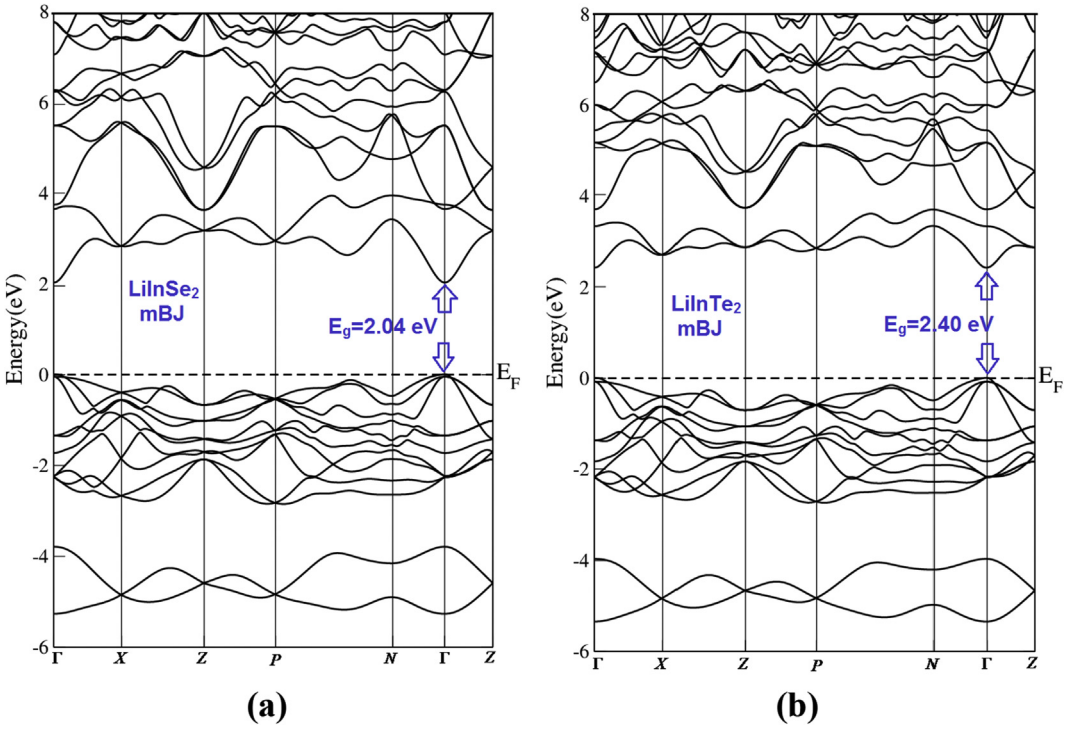

Fig. 2. Calculated electronic band structure using *mBJ* for; (a) $LiInSe_2$; (b) $LiInTe_2$.

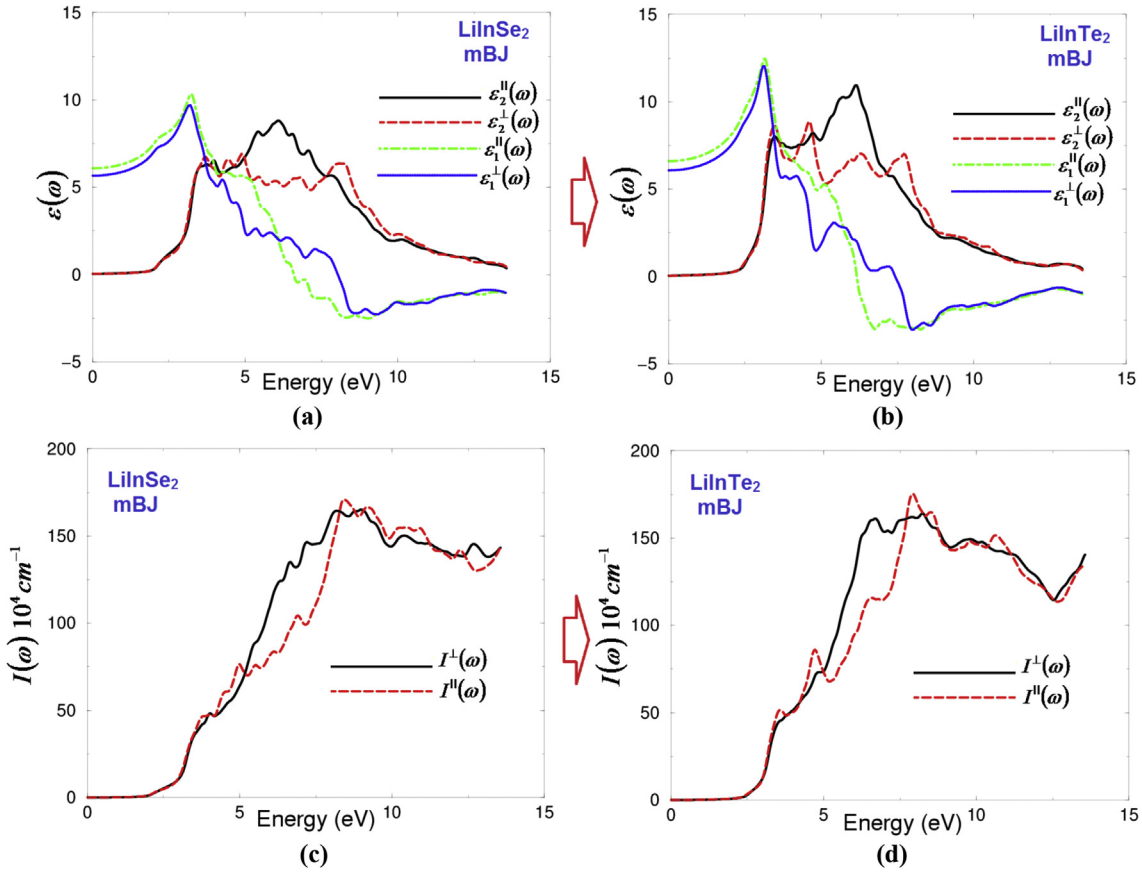

Fig. 3. **(a)** Calculated $\varepsilon_2^{\perp}(\omega)$ dispersion (dark solid curve-black), $\varepsilon_2^{II}(\omega)$ (light dashed curve-red) along with calculated $\varepsilon_1^{\perp}(\omega)$ (light dotted dashed curve -green), $\varepsilon_1^{II}(\omega)$ (light dotted curve -blue) for $LiInSe_2$ compound using *mBJ*; **(b)** Calculated $\varepsilon_2^{\perp}(\omega)$ dispersion (dark solid curve-black), $\varepsilon_1^{II}(\omega)$ (light dashed curve-red) along with calculated $\varepsilon_2^{\perp}(\omega)$ (light dotted dashed curve -green), $\varepsilon_1^{II}(\omega)$ (light dotted curve -blue) for $LiInTe_2$ compound using *mBJ*; **(c)** Calculated $I^{\perp}(\omega)$ (dark solid curve-black), $I^{II}(\omega)$ (light dashed curve-red) for $LiInSe_2$ compound using mBJ.; **(d)** Calculated $I^{\perp}(\omega)$ (dark solid curve-black), $I^{II}(\omega)$ (light dashed curve-red) for $LiInTe_2$ compound using *mBJ*. **(e)** Calculated $L^{\perp}(\omega)$ (dark solid curve-black), $L^{II}(\omega)$ (light dashed curve-red) for $LiInSe_2$ compound using mBJ.; **(f)** Calculated $L^{\perp}(\omega)$ (dark solid curve-black), $L^{II}(\omega)$ (light dashed curve-red) for $LiInTe_2$ compound using *mBJ*. **(h)** Calculated $n^{\perp}(\omega)$ (dark solid curve-black), $n^{II}(\omega)$ (light dashed curve-red) for $LiInSe_2$ compound using mBJ.; **(g)** Calculated $n^{\perp}(\omega)$ (dark solid curve-black), $n^{II}(\omega)$ (light dashed curve-red) for $LiInTe_2$ compound using *mBJ*. **(i)** Calculated $\Delta n(\omega)$(dark solid curve-black) for $LiInSe_2$, and (light dashed curve-red) for $LiInTe_2$. (For interpretation of the references to colour in this figure legend, the reader is referred to the web version of this article.)

nonlinear optical susceptibility tensor $\chi^{(2)}_{ijk}(-2\omega;\omega;\omega)$. These can be generally written as [34–37]:

$$\chi^{ijk}_{inter}(-2\omega;\omega,\omega)=\frac{e^3}{\hbar^2}\sum_{nml}\int\frac{d\vec{k}}{4\pi^3}\frac{\vec{r}^{\,i}_{nm}\left\{\vec{r}^{\,j}_{ml}\vec{r}^{\,k}_{ln}\right\}}{(\omega_{ln}-\omega_{ml})}\left\{\frac{2f_{nm}}{(\omega_{mn}-2\omega)}+\frac{f_{ml}}{(\omega_{ml}-\omega)}+\frac{f_{ln}}{(\omega_{ln}-\omega)}\right\} \tag{2}$$

$$\begin{aligned}\chi^{ijk}_{intra}(-2\omega;\omega,\omega)=\frac{e^3}{\hbar^2}\int\frac{d\vec{k}}{4\pi^3}\Bigg[&\sum_{nml}\omega_{nm}\vec{r}^{\,i}_{nm}\left\{\vec{r}^{\,j}_{ml}\vec{r}^{\,k}_{ln}\right\}\\&\times\left\{\frac{f_{nl}}{\omega^2_{ln}(\omega_{ln}-\omega)}-\frac{f_{lm}}{\omega^2_{ml}(\omega_{ml}-\omega)}\right\}-8i\\&\times\sum_{nm}\frac{f_{nm}\vec{r}^{\,i}_{nm}\left\{\Delta^j_{mn}\vec{r}^{\,k}_{nm}\right\}}{\omega^2_{mn}(\omega_{mn}-2\omega)}+2\\&\times\sum_{nml}\frac{f_{nm}\vec{r}^{\,i}_{nm}\left\{\vec{r}^{\,j}_{ml}\vec{r}^{\,k}_{ln}\right\}(\omega_{ml}-\omega_{ln})}{\omega^2_{mn}(\omega_{mn}-2\omega)}\Bigg]\end{aligned} \tag{3}$$

$$\begin{aligned}\chi^{ijk}_{mod}(-2\omega;\omega,\omega)=\frac{e^3}{2\hbar^2}\int\frac{d\vec{k}}{4\pi^3}\Bigg[&\\&\times\sum_{nml}\frac{f_{nm}}{\omega^2_{mn}(\omega_{mn}-\omega)}\left\{\omega_{nl}\vec{r}^{\,i}_{lm}\left\{\vec{r}^{\,j}_{mn}\vec{r}^{\,k}_{nl}\right\}-\omega_{lm}\vec{r}^{\,i}_{nl}\left\{\vec{r}^{\,j}_{lm}\vec{r}^{\,k}_{mn}\right\}\right\}-i\\&\times\sum_{nm}\frac{f_{nm}\vec{r}^{\,i}_{nm}\left\{\vec{r}^{\,j}_{mn}\Delta^k_{mn}\right\}}{\omega^2_{mn}(\omega_{mn}-\omega)}\Bigg]\end{aligned} \tag{4}$$

From these formulae we can notice that there are three major contributions to $\chi^{(2)}_{ijk}(-2\omega;\omega;\omega)$: the inter-band transitions $\chi^{ijk}_{inter}(-2\omega;\omega,\omega)$, the intra-band transitions $\chi^{ijk}_{intra}(-2\omega;\omega,\omega)$ and the modulation of inter-band terms by intra-band terms $\chi^{ijk}_{mod}(-2\omega;\omega,\omega)$, where $n\neq m\neq l$. Here n denotes the valence states, m the conduction states and l denotes all states($l\neq m,n$). There are two kinds of transitions that can take place, one of them denoted asvcc', involves one valence band (v) and two conduction bands (c and c'), and the second transition denoted as $vv'c$, involves two valence bands (v and v') and one conduction band (c). The symbols

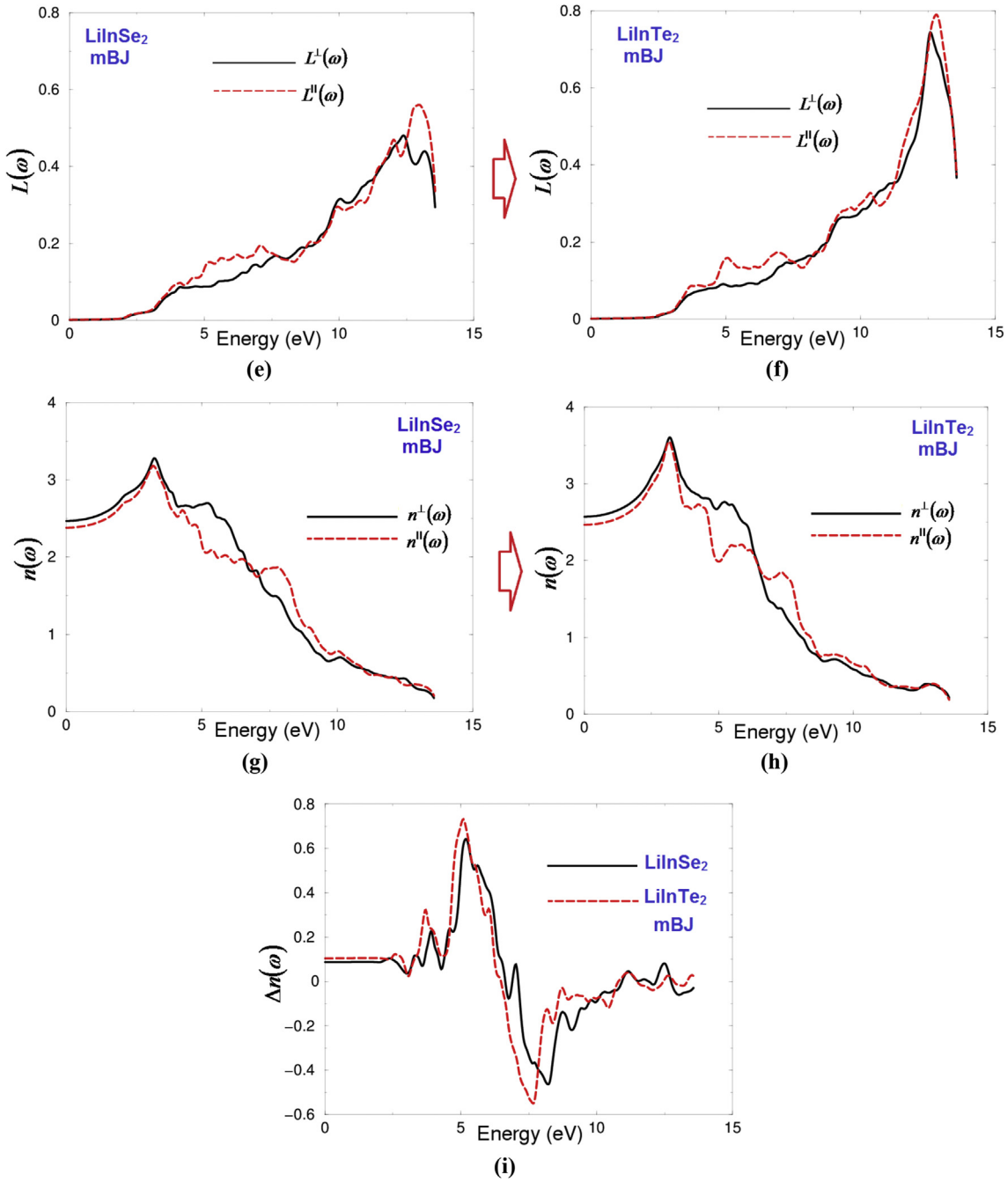

Fig. 3. (*Continued*)

are defined as $\Delta^i_{nm}(\vec{k}) = \vartheta^i_{nn}(\vec{k}) - \vartheta^i_{mm}(\vec{k})$ with $\vec{\vartheta}^i_{nm}$ being the i component of the electron velocity given as $\vartheta^i_{nm}(\vec{k}) = i\omega_{nm}(\vec{k})r^i_{nm}(\vec{k})$ and $\{r^i_{nm}(\vec{k})r^j_{ml}(\vec{k})\} = \frac{1}{2}(r^i_{nm}(\vec{k})r^j_{ml}(\vec{k}) + r^j_{nm}(\vec{k})r^i_{ml}(\vec{k}))$. The position matrix elements between band states n and m, $r^i_{nm}(\vec{k})$, are calculated from the momentum matrix element P^i_{nm} using the relation [38]: $r^i_{nm}(\vec{k}) = \frac{P^i_{nm}(\vec{k})}{im\omega_{nm}(\vec{k})}$, with the energy difference between the states n and m given by $\hbar\omega_{nm}=\hbar(\omega_n-\omega_m)$. $f_{nm}=f_n-f_m$ is the difference of the Fermi distribution functions. The i, j and k entries correspond to the Cartesian indices. It has been demonstrated by Aspnes [39] that only the one-electron virtual transitions (transitions between one valence band state and two conduction band states,vcc') give a significant contribution to the second-order tensor. We ignore the virtual-hole contribution (transitions between two valence band states and one conduction band state, $vv'c$), because it was found to be negative and more than an order of magnitude smaller than the virtual-electron contribution for this compound.

3. Results and discussion

3.1. Salient features of the electronic band structures

To ascertain the influence of substituting Se by Te on the electronic properties of $LiInX_2$ (X = Se, Te) single crystals, we have

Table 3
The calculated energy band gap of $LiInSe_2$ and $LiInTe_2$ in comparison with the experimental data [26,27] and the previous calculation [25] $\varepsilon_1^{\perp}(0)\varepsilon_1^{II}(0)\varepsilon_1^{average}(0)$, $\delta\varepsilon$, $\omega_p^{\perp}(\omega)$, $\omega_p^{II}(\omega)n^{\perp}(0)$, $n^{II}(0)$ and $\Delta n(0)$. In this work the parameters are calculated within mBJ.

	$LiInSe_2$	$LiInTe_2$
Eg (eV)	2.04*, 2.05[a], 1.684[c], 1.615[d]	2.40*, 2.41[b], 1.313[c], 1.513[d]
$\varepsilon_1^{\perp}(0)$	6.091	6.609
$\varepsilon_1^{II}(0)$	5.666	6.081
$\varepsilon_1^{tot}(0)$	11.757	12.690
$\delta\varepsilon$	−0.036	−0.041
$\omega_p^{\perp}(\omega)$	6.598	6.190
$\omega_p^{II}(\omega)$	8.040	7.442
$n^{\perp}(0)$	2.468	2.570
$n^{II}(0)$	2.380	2.466
$\Delta n(0)$	0.088	0.104

*This work.
[a] Ref. [32].
[b] Ref. [33].
[c] Ref. [31] GGA.
[d] Ref. [31] LDA.

calculated the electronic band structures using mBJ as shown in Fig. 2(a) and (b). It has been noticed that these materials posses direct energy band gap (Γ−Γ) of about 1.58 eV (LDA), 1.85 eV (GGA) and 2.04 eV (mBJ) for $LiInSe_2$, while the same band gaps are 1.76 eV (LDA), 1.92 eV (GGA) and 2.40 eV (mBJ) for $LiInTe_2$. It is clear that mBJ ensures much better agreement with the experimental band gaps (2.05 eV -$LiInSe_2$ and 2.41 eV -$LiInTe_2$) [26,27].

3.2. Complex first-order linear optical dispersion

Using Eq. (1) and following the dipolar selection rule which states that only those transitions, in which the angular momentum quantum number l is changed by unity ($\Delta=\pm1$) are allowed, we have calculated the imaginary and real parts of the optical dielectric functions for the $LiInX_2$ (X = Se, Te) single crystals using mBJ; the obtained results are shown in Fig. 3 (a) and 3 (b). It has been found that substituting Se by Te causes a shift of the whole spectral structure towards higher energies by around 0.36 eV with increasing the magnitude of the spectral structures. This result implies that the optical band gap is increased when we move from Se to Te in concordance with the calculated electronic band structure. The first absorption edges are located at 2.05 (2.41) eV for $LiInSe_2$ ($LiInTe_2$). These are due to optical transition between the Li-2s, In-5s, Se-4p (Te-5p) valence bands to the In-5s/5p, Se4s/4p (Te5s/5p) conduction bands. We observed that the spectral structure of $\varepsilon_2^{\perp}(\omega)$ for $LiInSe_2$ exhibits one main peak situated between

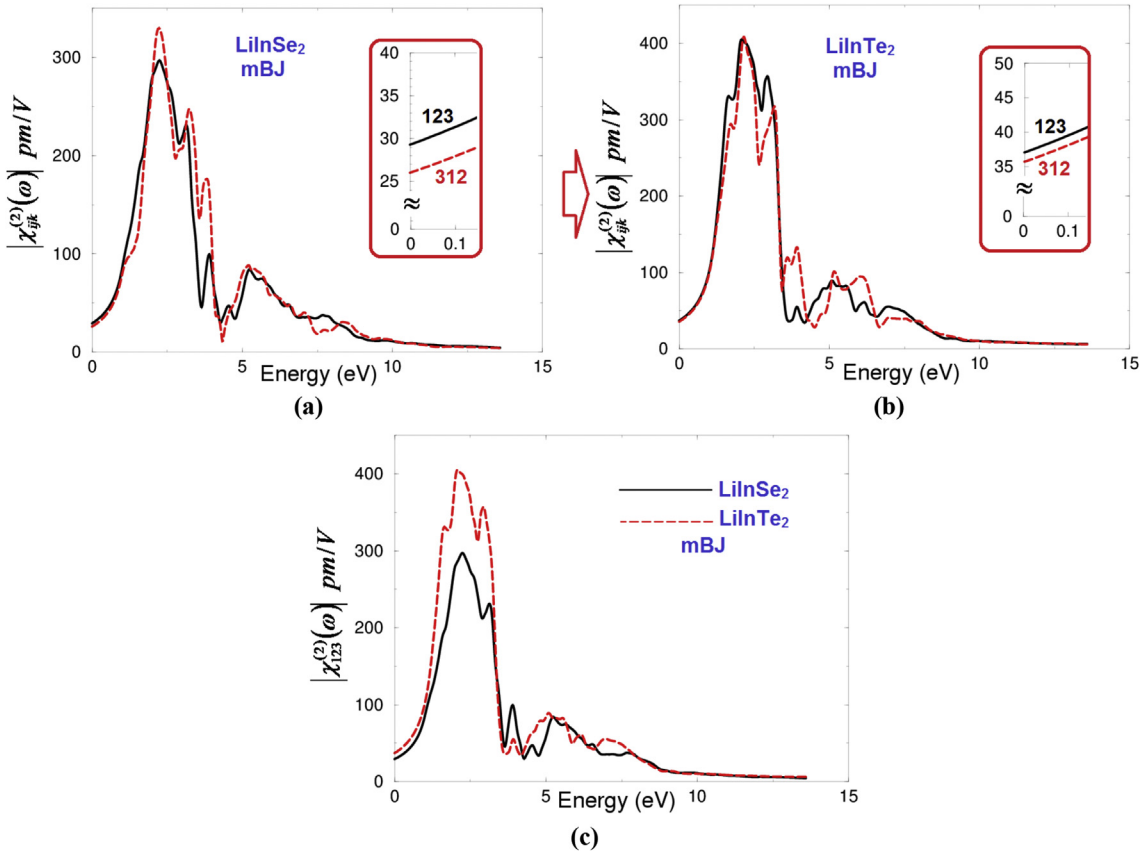

Fig. 4. **(a)** Calculated $\left|\chi_{ijk}^{(2)}(\omega)\right|$ for the two tensor components of $LiInSe_2$; **(b)** Calculated $\left|\chi_{ijk}^{(2)}(\omega)\right|$ for the five tensor components of $LiInTe_2$; **(c)** Calculated Imaginary $\chi_{123}^{(2)}(\omega)$(dark solid curve-black) and real $\chi_{123}^{(2)}(\omega)$ (light dashed curve-red) spectra of $LiInSe_2$; **(d)** Calculated Imaginary $\chi_{333}^{(2)}(\omega)$(dark solid curve-black) and real $\chi_{333}^{(2)}(\omega)$ (light dashed curve-red) spectra of $LiInTe_2$; **(e)** Calculated total $\mathrm{Im}\chi_{123}^{(2)}(\omega)$ spectrum (dark solid curve-black) along with the intra $(2\omega)/(1\omega)$ (light solid curve-blue)/(light dashed doted curve-cyan) and inter $(2\omega)/(1\omega)$ (light long dashed curve-red)/(light doted curve-green) -band contributions of $LiInSe_2$, here all $\mathrm{Im}\chi_{123}^{(2)}(\omega)$ are multiplied by 10^{-7}, in esu units; **(f)** Calculated total $\mathrm{Im}\chi_{123}^{(2)}(\omega)$ spectrum (dark solid curve-black) along with the intra $(2\omega)/(1\omega)$ (light solid curve-blue)/(light dashed doted curve-cyan) and inter $(2\omega)/(1\omega)$ (light long dashed curve-red)/(light doted curve-green) -band contributions of $LiInTe_2$, here all $\mathrm{Im}\chi_{123}^{(2)}(\omega)$ are multiplied by 10^{-7}, in esu units; **(g)** −***upper panel-*** Calculated $\left|\chi_{123}^{(2)}(\omega)\right|$(dark solid curve-black); ***-lower panel-*** Calculated $\varepsilon_2^{xx}(\omega)$ (dark solid curve-black); Calculated $\varepsilon_2^{xx}(\omega/2)$ (dark dashed curve-red) of $LiInSe_2$; **(h)** −***upper panel-*** Calculated $\left|\chi_{123}^{(2)}(\omega)\right|$(dark solid curve-black); ***-lower panel-*** Calculated $\varepsilon_2^{xx}(\omega)$ (dark solid curve-black); Calculated $\varepsilon_2^{xx}(\omega/2)$ (dark dashed curve-red) of $LiInTe_2$. (For interpretation of the references to colour in this figure legend, the reader is referred to the web version of this article.)

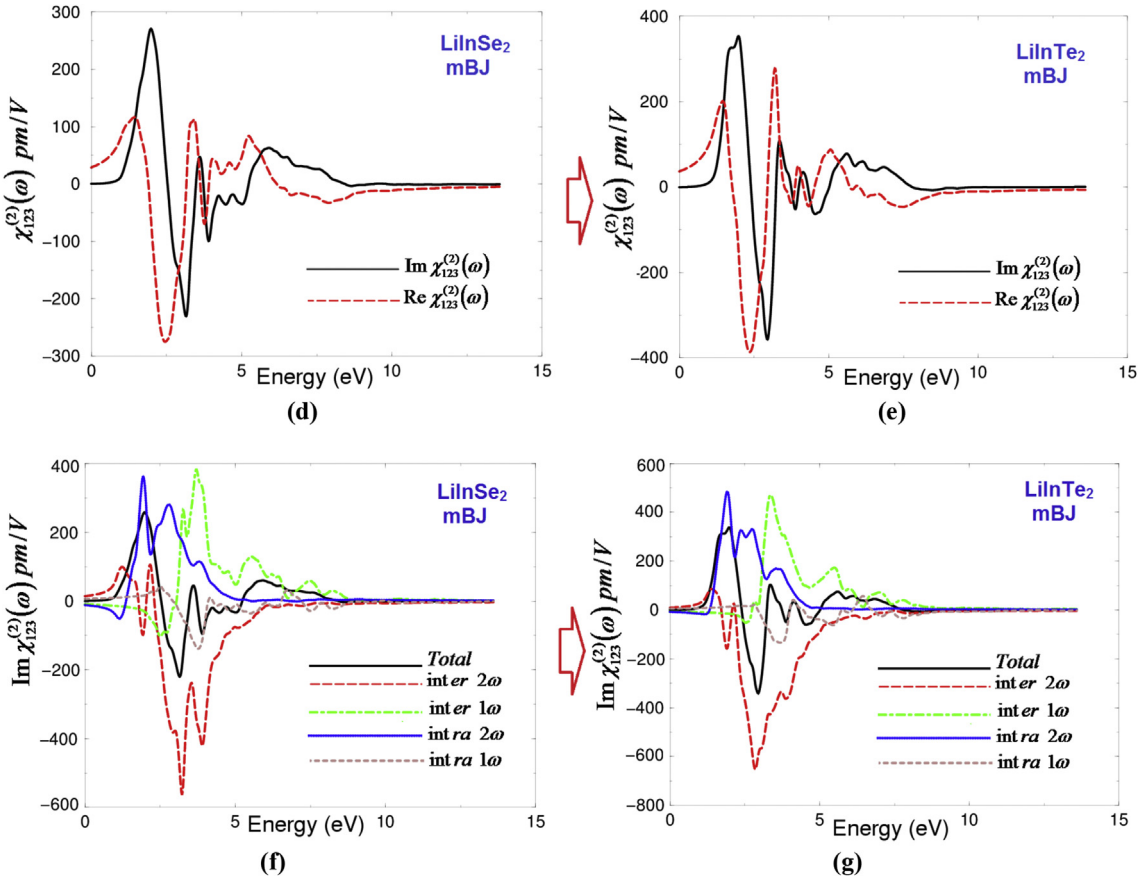

Fig. 4. (**Continued**)

two humps, whereas $\varepsilon_2^{II}(\omega)$ show multi humps in the main structure. At the same time, the $\varepsilon_2^{\perp}(\omega)$ for $LiInTe_2$ shows one main peak and two humps located at the left side of the main peak, whereas $\varepsilon_2^{II}(\omega)$ exhibit multi peaks in the main structure. The main spectral structures are due to the optical transitions between the Li-2s, In5s/5p, Se-4p (Te-5p) valence bands to Li-2s, In-5s/5p, Se-4s/4p (Te-5s/5p) conduction bands. The strength of the main peaks could be explained by the fact that $\varepsilon_2(\omega)$ scales as $1/\omega^2$.

From the calculated real part $\varepsilon_1^{\perp}(\omega)$ and $\varepsilon_1^{II}(\omega)$ we have obtained the vanishing frequency value of the dielectric function, which defines the static electronic dielectric constant $\varepsilon_1^{\perp}(0)$ and $\varepsilon_1^{II}(0)$. These values are listed in Table 3. Using these values we can estimate the energy gap from the Penn model [40], $\varepsilon(0) \approx 1 + (\hbar\omega_P/E_g)^2$. It is clear that $\varepsilon(0)$ is inversely proportional to E_g therefore, smaller $\varepsilon(0)$ would correspond to larger E_g. Following Table 3 it has been found that the value of $\varepsilon(0)$ for $LiInSe_2 > LiInTe_2$. This is another evidence that moving from Se to Te in $LiInX_2$ increases the band gap. Furthermore, the $\varepsilon(0)$ values help to estimate the uniaxial anisotropy as listed in Table 3. From the real parts of the dielectric function we can obtain the plasmon oscillations $\omega_p^{\perp}(\omega)$ and $\omega_p^{II}(\omega)$ (Table 3), which occur at energy where $\varepsilon_1(\omega)$ crosses zero. It is associated with the existence of plasma oscillations (plasmons). With the aid of existing information about $\varepsilon_1(\omega)$ and $\varepsilon_2(\omega)$, the other optical properties can be calculated. The absorption coefficients of $LiInSe_2$ and $LiInTe_2$ as illustrated in Fig. 3(c) and (d) indicate that the absorption edges occur at 2.04 eV and 2.40 eV in concordance with our observation from $\varepsilon_2(\omega)$ (Fig. 3(a) and (b)) that the energy band gap enlargement occurs when we substituting Se by Te. It has been noticed that $LiInSe_2$ and $LiInTe_2$ posses relatively wide optical transparency region.

Fig. 3(e) and (f) show the energy loss function $L(\omega)$ of $LiInSe_2$ and $LiInTe_2$, the lossless region of $LiInSe_2$ is confined between 10.0 eV and 13.0 eV, whereas it is between 11.0 eV and 14.0 eV for $LiInTe_2$. There are some other features in the $L(\omega)$ behavior, in addition to the plasmon peak, associated with the interband transitions. The most intensive feature is the plasmon peak, it occurs at energy region where $\varepsilon_1(\omega)$ goes to zero. In Fig. 3(g) and (h) the calculated refractive indices of $LiInSe_2$ and $LiInTe_2$ are plotted, the values of $n^{\perp}(0)$ and $n^{II}(0)$ were calculated and presented in Table 3. From the calculated refractive indices we can estimate the birefringence from the following expression $\Delta n(\omega) = n_e(\omega) - n_o(\omega)$. It has been found that both compounds exhibit positive birefringence at the static limit as shown in Table 3. The birefringence is necessary to fitful the phase-matching condition. The dispersion of the birefringence of the two compounds is illustrated in Fig. 3(i).

3.3. Complex second-order non-linear optical dispersion

It has been reported that the materials, which show a considerable anisotropy in the linear optical susceptibilities, favor an enhanced phase matching conditions for the second harmonic generation (SHG) and optical parametric oscillation (OPO). Also the materials with a wide band gap posses high laser damage threshold [41,42]. It is clear that from the calculated linear optical properties both $LiInSe_2$ and $LiInTe_2$ exhibit a considerable anisotropy between the two optical components. As a result, these materials are expected to produce strong SHG. Furthermore the calculated electronic band structure reveals that these compounds possess a wide energy band gap and hence they exhibit high laser damage threshold. In this section we turn our concern to calculate the

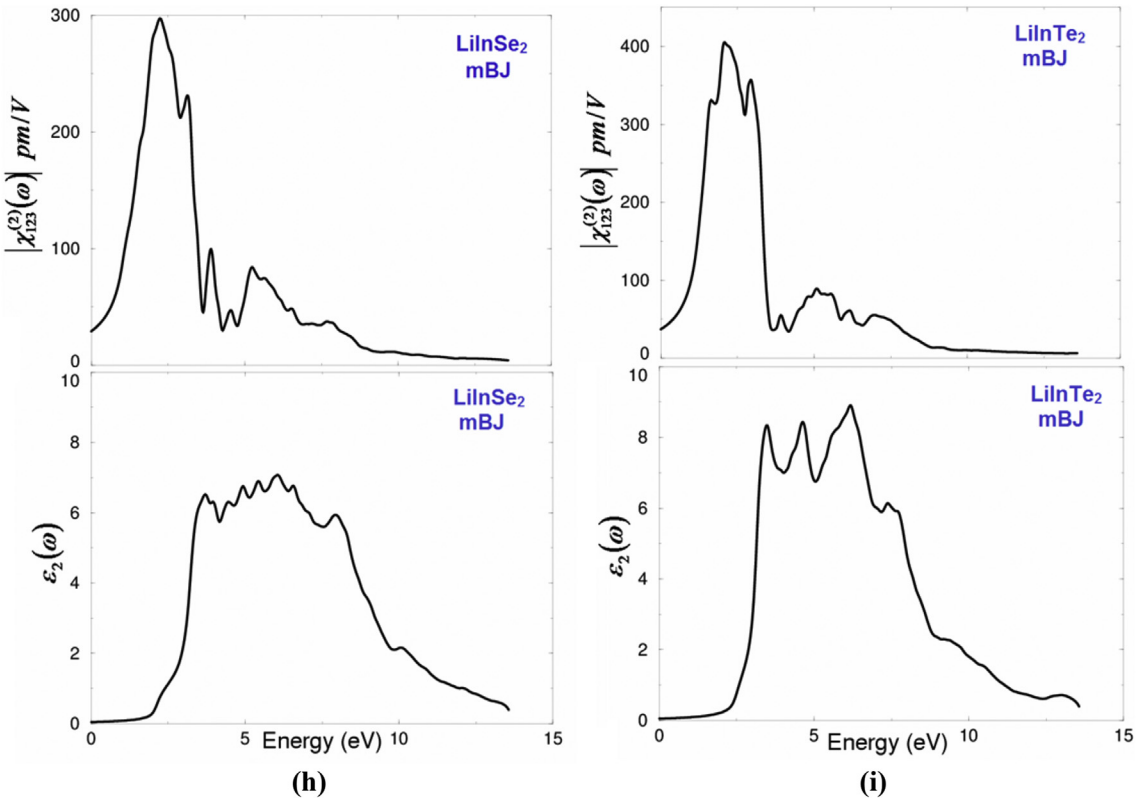

Fig. 4. (*Continued*)

Table 4
Calculated $\left|\chi^{(2)}_{ijk}(\omega)\right|$ of $LiInSe_2$, in pm/V at static limit and at $\lambda = 1064$ nm, in comparison with the experimental value of the well known $KTiOPO_4$ (KTP) single crystals which exhibits a SHG value of about 16.9 [43], 13.7 [44], 15.4 ± 0.2 [45], 14.6 ± 1.0 [46], 17.4 ± 1.7 [47], 16.9 ± 3.3 [48], 16.9 ± 1.7 [49], 10.6 ± 7.5 [50], 16.75 [51] and 16.65 [51] at $\lambda = 1064$. Where 1 pm/V = 2.387×10^{-9} esu.

$LiInSe_2$				
Tensor components	$\chi^{(2)}_{ijk}(0)$	Theory $d_{ijk} = 0.5\chi^{(2)}_{ijk}(\omega)$	$\chi^{(2)}_{ijk}(\omega)$ at $\lambda = 1064$	Theory $d_{ijk} = 0.5\chi^{(2)}_{ijk}(\omega)$
$\left\|\chi^{(2)}_{123}(\omega)\right\|$	29.177	$d_{14} = 14.588$	111.465	$d_{14} = 55.732$
$\left\|\chi^{(2)}_{312}(\omega)\right\|$	26.002	$d_{36} = 13.001$	95.861	$d_{36} = 47.930$

complex second-order non-linear optical properties of $LiInSe_2$ and $LiInTe_2$ single crystals.

Since both $LiInSe_2$ and $LiInTe_2$ single crystals are crystallized in tetragonal symmetry, only two non-zero tensor components $\chi^{(2)}_{123}(-2\omega;\omega;\omega)$ and $\chi^{(2)}_{312}(-2\omega;\omega;\omega)$ are allowed. The calculated absolute values of $\left|\chi^{(2)}_{123}(-2\omega;\omega;\omega)\right|$ and $\left|\chi^{(2)}_{312}(-2\omega;\omega;\omega)\right|$ for both compounds reveal that the $\left|\chi^{(2)}_{123}(-2\omega;\omega;\omega)\right|$ component is the dominant one (Fig. 4(a) and (b)). It has been found that $LiInTe_2$ exhibits higher SHG than that one obtained from $LiInSe_2$. These values are listed in Tables 4 and 5. We also found that $LiInSe_2$ ($LiInTe_2$) exhibit a SHG of about seven (nine) times than that the experimental value of the well known $KTiOPO_4$ (KTP) single crystals. We would like to mention that the experimental value of the SHG signal for the well known $KTiOPO_4$ (KTP) single crystals of about 16.9 [43], 13.7 [44], 15.4 ± 0.2 [45], 14.6 ± 1.0 [46], 17.4 ± 1.7 [47], 16.9 ± 3.3 [48], 16.9 ± 1.7 [49], 10.6 ± 7.5 [50], 16.75 [51] and 16.65 [51].

Further detailed information regarding the origin of the strong SHG for the two compounds can be obtained from analyzing the real and imaginary parts of the dominant component $\chi^{(2)}_{123}(-2\omega;\omega;\omega)$ as shown in Fig. 4(c) and (d). It has been found that the 2ω terms begin to oscillate at the half value of the energy band gap, whereas the ω terms oscillate at the exact value of the fundamental gap to be added to 2ω terms. Both of 2ω and ω terms

Table 5
Calculated $\left|\chi^{(2)}_{ijk}(\omega)\right|$ of $LiInTe_2$ in pm/V at static limit and at $\lambda = 1064$ nm, in comparison with the experimental value of the well known $KTiOPO_4$ (KTP) single crystals which exhibits a SHG value of about 16.9 [43], 13.7 [44], 15.4 ± 0.2 [45], 14.6 ± 1.0 [46], 17.4 ± 1.7 [47], 16.9 ± 3.3 [48], 16.9 ± 1.7 [49], 10.6 ± 7.5 [50], 16.75 [51] and 16.65 [51] at $\lambda = 1064$. Where 1 pm/V = 2.387×10^{-9} esu.

$LiInTe_2$				
Tensor components	$\chi^{(2)}_{ijk}(0)$	Theory $d_{ijk} = 0.5\chi^{(2)}_{ijk}(\omega)$	$\chi^{(2)}_{ijk}(\omega)$ at $\lambda = 1064$	Theory $d_{ijk} = 0.5\chi^{(2)}_{ijk}(\omega)$
$\left\|\chi^{(2)}_{123}(\omega)\right\|$	37.058	$d_{14} = 18.529$	140.73	$d_{14} = 70.365$
$\left\|\chi^{(2)}_{312}(\omega)\right\|$	35.646	$d_{36} = 17.823$	136.917	$d_{36} = 68.458$

are further separate to inter- and intra band transtions as illustrated in Fig. 4(e) and (f).

To identify the origin of the spectral peaks as caused by the $2\omega/\omega$ inter-intra-band contributions, we have associated the spectral structures of the dominant component to the absorptive part of the optical dielectric function $\varepsilon_2(\omega)$ as a function of both $\omega/2$ and ω as shown in Fig. 4(g) and (h). The first structure in $\left|\chi^{(2)}_{123}(\omega)\right|$ between 1.02 and 2.05 eV (1.20–2.41 eV) for $LiInSe_2$ ($LiInTe_2$) is mainly originated from the 2ω resonance. The second structure between 2.05 and 5.0 eV (2.41–5.0 eV) is associated with interference between 2ω andω resonances (the absorption edge of $\varepsilon_2(\omega)$). The last spectral structure from 5.0 eV and above is mainly due to ω resonance and is associated with the second structure in $\varepsilon_2(\omega)$.

4. Conclusions

We have optimized the experimental lattice parameters of two $LiInX_2$ (X = Se, Te) chalcopyrite crystals using the all-electron full potential linear augmented plane wave plus local orbitals (FPLAPW + lo) method in a scalar relativistic version as embodied in the WIEN2k code. The exchange and correlation potentials were described by local density approximation (LDA), the generalized gradient approximation (PBE-GGA) and the recently modified Becke-Johnson potential (mBJ). The complex first-order linear optical dispersion and complex second-order non-linear optical dispersion of the $LiInX_2$ (X = Se, Te) single crystals were calculated based on density functional theory. Calculations show that these materials posses direct energy band gap (Γ–Γ) of about 1.58 eV (LDA), 1.85 eV (GGA) and 2.04 eV (mBJ) for $LiInSe_2$. While it is 1.76 eV (LDA), 1.92 eV (GGA) and 2.40 eV (mBJ) for $LiInTe_2$. The mBJ method is better to be used for getting the calculated band gaps to be closer to the experimental ones (2.05 eV -$LiInSe_2$ and 2.41 eV -$LiInTe_2$). It has been found that both compounds exhibit negative uniaxial anisotropy and positive birefringence at the static limit. To identify the origin of the spectral peaks as caused by $2\omega/\omega$ inter-intra-band contributions, we have associated the spectral structures of the dominant component to the absorptive part of the optical dielectric function $\varepsilon_2(\omega)$ as a function of both $\omega/2$ and ω. It has been found that $LiInTe_2$ exhibit a higher SHG signal than that obtained from $LiInSe_2$. We found that $LiInSe_2$ ($LiInTe_2$) exhibit a SHG of about seven (nine) times than that the experimental value of the well known $KTiOPO_4$ (KTP) single crystals.

Acknowledgments

The result was developed within the CENTEM project, reg. no. CZ.1.05/2.1.00/03.0088, cofunded by the ERDF as part of the Ministry of Education, Youth and Sports OP RDI programme and, in the follow-up sustainability stage, supported through CENTEM PLUS (LO1402) by financial means from the Ministry of Education, Youth and Sports under the "National Sustainability Programme I. Computational resources were provided by MetaCentrum (LM2010005) and CERIT-SC (CZ.1.05/3.2.00/08.0144) infrastructures. M.G. Brik acknowledges the Recruitment Program of High-end Foreign Experts (Grant No. GDW20145200225), the Programme for the Foreign Experts offered by Chongqing University of Posts and Telecommunications, European Regional Development Fund (Center of Excellence 'Mesosystems: Theory and Applications', TK114), Marie Curie Initial Training Network LUMINET, Grant agreement No. 316906, and the Ministry of Education and Research of Estonia, Project PUT430.

References

[1] S.K. Deb, A. Zunger (Eds.), Ternary and Multinary Compounds, Materials Research Society, Pittsburgh, Pennsylvania, 1987.
[2] G.E. Jaffe, A. Zunger, Phys. Rev. B 28 (1983) 5822v, 29, 1882(1984).
[3] C. Rincon, C. Bellabarba, Phys. Rev. B 33 (1986) 7160.
[4] E. Parthe, Crystal Chemistry of Tetrahedral Structures, Gordon and Breach, New York, 1964.
[5] N.A. Goryunova, The Chemistry of Diamond-like Semiconductors, Chapman and Hall, New York, 1965.
[6] J.L. Shay, J.H. Wernick, Ternury Chalcopyrite Semiconductors: Growth, Electronic Properties and Applications, Oxford, Pergamon, 1974.
[7] U. Kaufmann, J. Schneider, in: J. Treusch (Ed.), Festkorperprobleme XIV, Vieweg, Braunschweig, 1974, p. 229.
[8] Wagner, in: J.O. Pankove (Ed.), Electroluminescence, Springer, Berlin, 1977, p. 171.
[9] A. Mackinnon, in: J. Treusch (Ed.), Festkorperprobleme XXI, Vieweg Dortmund, 1981, p. 149.
[10] A. Miller, A. Mackinnon, D. Weaire, in: H. Ehrenreich, F. Seitz, D. Turubull (Eds.), Solid State Physics, 36, Academic, New York, 1981.
[11] B.R. Pamplin, T. Kiyosawa, K. Mastumoto, Prog. Cryst. Growth Charact. 1 (1979) 331.
[12] L.L. Kazmerski, Nuovo Cimento, D2, 2013, 1983.
[13] J.L. Shay, L.M. Schiavone, E. Buehier, J.H. Wernick, J. Appl. Phys. 43 (1972) 2805;
[a] S. Wagner, J.L. Shay, B. Tell, H.M. Kasper, Appl. Phys. Lett. 22 (1973) 351.
[14] B.F. Levine, Phys. Rev. B 7 (1973) 2600 (and references therein).
[15] F.K. Hopkius, Laser Focus World 31 (1995) 87.
[16] I. Repins, M.A. Contreras, B. Egaas, C. DeHart, J. Scharf, C.L. Perkins, B. To, R. Noufi, Prog. Photovolt. Res. Appl. 18 (2008) 235.
[17] M. Magesh, A. Arunkumar, P. Vijayakumar, G. Anandha Babu, P. Ramasamy, Opt. Laser Technol. 56 (2014) 177.
[18] Y.L. Li, W.L. Fan, H.G. Sun, X.F. Cheng, P. Li, X. Zhao, J. Appl. Phys. 106 (2009) 033704.
[19] A.V. Kosobutsky, YuM. Basalaev, Solid State Commun. 199 (2014) 17.
[20] T.-H. Ma, C.-H. Yang, Y. Xie, L. Sun, W.-Q. Lv, R. Wang, C.-Q. Zhu, M. Wang, Comput. Mater. Sci. 47 (2009) 99.
[21] T.-H. Ma, L. Sun, C. Xu, Y.F. Chen, J. Alloys Compd. 509 (2011) 9733;
[b] T.-H. Ma, Z.-P. Zhuang, Y.-L. Ren, Acta Phys. Sin.. 61 (2012) 197101.
[22] A.V. Kosobutsky, YuM. Basalaev, J. Phys. Chem. Solids 71 (2010) 854.
[23] A.V. Kosobutsky, YuM. Basalaev, A.S. Poplavnoi, Phys. Status Solidi B 246 (2009) 364.
[24] B. Lagoun, T. Bentria, B. Bentria, Comput. Mater. Sci. 68 (2013) 379.
[25] C.-G. Ma, M.G. Brik, Solid State Commun. 203 (2015) 69.
[26] H.J. Beister, S. Ves, W. Hönle, K. Syassen, G. Kühn, Phys. Rev. B 43 (1991) 9635.
[27] W. Hönle, G. Kühn, H. Neumann, Zeit. Annorg. Allg. Chem. 532 (1986) c0.
[28] J.P. Perdew, A. Zunger, Phys. Rev. B 23 (1981) 5048.
[29] J.P. Perdew, K. Burke, M. Ernzerhof, Phys. Rev. Lett. 77 (1996) 3865–3868.
[30] P. Blaha, K. Schwarz, G.K.H. Madsen, D. Kvasnicka, J. Luitz, WIEN2k, an Augmented Plane Wave Plus Local Orbitals Program for Calculating Crystal Properties, Vienna University of Technology, Austria, 2001.
[31] F. Tran, P. Blaha, Phys. Rev. Lett. 102 (2009) 226401.
[32] F. Bassani, G.P. Parravicini, Electronic States and Optical Transitions in Solids, Pergamon Press Ltd., Oxford, 1975, pp. p149–154.
[33] F. Wooten, Optical Properties of Solids, Academic press New York, USA, 1972.
[34] S. Sharma, J.K. Dewhurst, C. Ambrosch-Draxl, Phys. Rev. B 67 (2003) 165332.
[35] A.H. Reshak, Ph.D. Thesis, Indian Institute of Technology-Rookee, India, 2005.
[36] A.H. Reshak, J. Chem. Phys. 125 (014708) (2006).
[37] A.H. Reshak, J. Chem. Phys. 124 (014707) (2006).
[38] C. Ambrosch-Draxl, J. Sofo, Comp. Phys. Commun. 175 (2006) 1–14.
[39] D.E. Aspnes, Phys. Rev. B 6 (1972) 4648.
[40] D.R. Penn, Phys. Rev. B 128 (1962) 2093.
[41] J.W. Lekse, M.A. Moreau, K.L. McNerny, J. Yeon, P.S. Halasyamani, J.A. Aitken, Inorg. Chem. 48 (2009) 7516–7518.
[42] A.G. Jackson, M.C. Ohmer, S.R. LeClair, Infrared Phys. Technol. 38 (1997) 233–244.
[43] K. Zhang, X. Wang, Chin. Sci. Bull. 46 (2001) 2028–2036.
[44] http://www.castech-us.com/casktp.htm.
[45] M.V. Pack, D.J. Armstrong, A.V. Smith, Appl. Opt. 43 (2004) 3319.
[46] I. Shoji, T. Kondo, A. Kitamoto, M. Shirane, R.J. Ito, Opt. Soc. Am. B 14 (1997) 2268–2294.
[47] A. Anema, T. Rasing, Appl. Opt. 36 (1997) 5902–5904.
[48] L.K. Cheng, L.T. Cheng, J. Galperin, P.A.M. Hotsenpiller, J.D.J. Bierlein, Cryst. Growth 137 (1994) 107–115.
[49] H. Vanherzeele, J.D. Bierlein, Opt. Lett. 17 (1992) 982–984.
[50] B. Boulanger, J.P. Feve, G. Marnier, B. Menaert, Pure Appl. Opt. 7 (1998) 239.
[51] A.H. Reshak, I.V. Kityk, S.J. Auluck, Phys. Chem. B 114 (2010) 16705–16712.